Inactivation of AMPK leads to attenuation of antigen presentation and immune evasion in lung adenocarcinoma

Yajing Gao, Pekka Päivinen, Sushil Tripathi, Eva Domenech-Moreno, Iris Wong, Kari Vaahtomeri, Ashwini Nagaraj, Sarang Talwelkar, Marc Foretz, Emmy Verschuren, et al.

Inactivation of AMPK leads to attenuation of antigen presentation and immune evasion in lung adenocarcinoma

Yajing Gao[1,7#], Pekka Päivinen[1,2#], Sushil Tripathi[1,2#], Eva Domenech-Moreno[1,2], Iris P.L. Wong[1], Kari Vaahtomeri[3], Ashwini S. Nagaraj[4], Sarang S. Talwelkar[4], Marc Foretz[5], Emmy W. Verschuren[4], Benoit Viollet[5], Yan Yan[1,6*], Tomi P. Mäkelä[1,2]

[1] iCAN Digital Precision Cancer Medicine Flagship and

[2] HiLIFE-Helsinki Institute of Life Science, University of Helsinki, Finland

[3] Translational Cancer Medicine Research Program, Faculty of Medicine, University of Helsinki and Wihuri Research Institute, Finland

[4] Institute for Molecular Medicine Finland (FIMM), HiLIFE, University of Helsinki, Helsinki, Finland

[5] Université de Paris, Institut Cochin, CNRS, INSERM, Paris, France

[6] Current address: Cancer Biology & Genetics Program, Sloan Kettering Institute, Memorial Sloan Kettering Cancer Center, New York, USA

[7] Current address: Colorectal Service, Department of Surgery, Memorial Sloan Kettering Cancer Center, New York, USA

#These authors contributed equally to this work.

Corresponding author: Yan Yan, Zuckerman Research Center, 417 East 68th Street, Room ZRC-1331, New York, New York 10065. Email: yany@mskcc.org

Running title: Inactivation of AMPK leads to immune evasion in lung cancer.

Authors' disclosures:

Y. Gao is supported by Sigrid Juselius Foundation. Sushil Tripathi was supported by Academy of Finland postdoc fellowship and Instrumentarium Science Foundation. Y. Yan reports grants from Sigrid Juselius Foundation, Finnish Cultural Foundation, Maud Kuistila Memorial Foundation, Biomedicum Helsinki Foundation, Cancer Society of Finland, Paulo Foundation, University of Helsinki, Ida Montinin Foundation, K. Albin Johanssons Foundation, Instrumentarium Science Foundation and Otto A. Malm Foundation. EW Verschuren reports grants from European Union's Seventh Framework Programme and Academy of Finland. T.P. Mäkelä reports grants from Sigrid Juselius Foundation, Finnish Cancer Organizations, and Academy of Finland as well as personal fees from the European Commission outside the submitted work.

Conflicts of interest: The authors declare no potential conflicts of interest.

Word count: 5234; total number of figures and tables: 5.

Statement of Translational relevance: *LKB1* inactivation in NSCLC is clinically relevant as it leads to resistance to immune checkpoint inhibitors. The findings of this study provide evidence that this immune evasion is due to subsequent inactivation of AMPK and attenuation of antigen presentation and suggest that restoration of AMPK activity could increase the number of patients benefiting from immunotherapy. Furthermore, the study expands the correlation between immune evasion and *LKB1* mutations to include a larger number of NSCLC without detectable LKB1 mutation.

Abstract

Purpose: Mutations in *STK11 (LKB1)* occur in 17% of lung adenocarcinoma (LUAD) and drive a suppressive (cold) tumor immune microenvironment (TIME) and resistance to immunotherapy. The mechanisms underpinning the establishment and maintenance of a cold TIME in *LKB1* mutant LUAD remain poorly understood. In this study, we investigated the role of the LKB1 substrate AMPK in immune evasion in human NSCLC and mouse models and explored the mechanisms involved.

Experimental Design: We addressed the role of AMPK in immune evasion in NSCLC by correlating AMPK phosphorylation and immune suppressive signatures and by deleting *AMPKα1 (Prkaa1)* and *AMPKα2 (Prkaa2)* in a $Kras^{G12D}$-driven LUAD. Furthermore, we dissected the molecular mechanisms involved in immune evasion by comparing gene expression signatures, AMPK activity, and immune infiltration in mouse and human LUAD and gain or loss of function experiments with LKB1- or AMPK-deficient cell lines.

Results: Inactivation of both AMPKα1 and AMPKα2 together with Kras activation accelerated tumorigenesis and led to tumors with reduced infiltration of $CD8^+$/$CD4^+$ T cells and gene signatures associated with a suppressive TIME. These signatures recapitulate those in *Lkb1*-deleted murine LUAD and in *LKB1*-deficient human NSCLC. Interestingly a similar signature is noted in human NSCLC with low AMPK activity. In mechanistic studies we find that compromised LKB1 and AMPK activity leads to attenuated antigen presentation in both LUAD mouse models and human NSCLC.

Conclusions: The results provide evidence that the immune evasion noted in *LKB1* inactivated lung cancer is due to subsequent inactivation of AMPK and attenuation of antigen presentation.

Introduction

STK11/LKB1 mutations represent a challenge in non-small cell lung cancer (NSCLC) occurring in 17%-23% of NSCLC adenocarcinomas (1) often together with *KRAS*-activating mutations. Importantly, the presence of *LKB1* mutations or reduction of LKB1 expression in lung cancer patients associates with a more aggressive clinical phenotype (2) and resistance to conventional chemotherapy (3) as well as target therapies inhibiting either downstream effectors of KRAS signaling (4), suggesting novel therapeutic strategies are needed to target this subset of lung cancers. PD-1/PD-L1 checkpoint blockade immunotherapy elicits durable antitumor effects in multiple cancers including NSCLC, yet not all patients respond. Retrospective studies in four independent cohorts identified genomic alterations of *STK11/LKB1* as a major driver of immune escape and tumor cell-intrinsic determinant of primary resistance to PD-1/PD-L1 blockade in NSCLC, despite the presence of intermediate or high tumor mutation burden (5). Consistently, a pan-tumor analysis of genomic markers associated with anti-PD-1 response demonstrated that tumor mutation burden (TMB) and a T cell-inflamed gene expression profile (GEP) can jointly stratify cancer patients into groups with different response to PD-1 blockade, with *LKB1* mutation in LUAD identified to have the most significant negative associations with T cell-inflamed GEP across 20 cancer types (6). These findings are recapitulated in a genetically engineered mouse model (GEMM) of lung cancer driven by oncogenic *Kras* mutation ($Kras^{G12D}$) where Lkb1 inactivation leads to accelerated tumor growth (7), metastatic potential (7) and suppressed T-cell activity in the tumor immune microenvironment (TIME) (8).

STK11/LKB1 encodes a serine/threonine kinase activating at least 14 related kinases including AMPK*s,* NUAK*s,* MARK*s,* SIK*s* and BRSK*s* and thereby regulates several cellular processes including cell metabolism, cell polarity, and growth (9). Using CRISPR/Cas9-mediated deletion

of these substrates, SIK1-3 deletion was noted to recapitulate the accelerated growth noted after *Lkb1* deletion in the $Kras^{G12D}$ GEMM model (10, 11). The substrate(s) mediating effects on the tumor microenvironment and checkpoint inhibitor responses however remain to be identified.

The widely used antidiabetic drug metformin can reprogram the tumor microenvironment in lung cancer (12), esophageal squamous cell carcinoma (13) and colorectal cancer (14). As metformin also activates the LKB1 substrate AMPK (15), we hypothesized that inactivation of AMPK may contribute to the suppressive TIME in LKB1 deficient tumors. To address this, we investigated the association with AMPK activity and immune suppression in human lung cancer and generated GEMM models enabling inactivation of AMPK simultaneously with activation of *Kras* to investigate the causal role of AMPK in immune evasion.

Materials and Methods

Mice. All the experimental mouse strains (below) were generated from *Kras*$^{LSL\text{-}G12D/+}$(16), *Lkb1*$^{flox/flox}$ (17), *AMPKa1*$^{fl/fl}$ and *AMPKa2*$^{fl/fl}$ (a kind gift from Benoit Violet) mice. The mice are in mixed genetic background of C57BL/6J and CD-1. All experiments utilized a mixture of female and male mice. Mice aged about 8-10 weeks were intranasally instilled with Ad5-CMV-Cre ($5x10^7$ PFUs, University of Kupio, Finland) or Ad5-SPC-Cre (2.5x109 PFUs) in 50µl MEM per mouse following the protocol previously described (18). Animals were housed in a pathogen-free facility at the Laboratory Animal Center of the University of Helsinki. Animal studies have been approved by the Finnish National Experiment Board (ESAVI/2327/04.10.07/2017).

Human lung cancer specimens. Surgically resected tumor specimens were received from NSCLC patients at the Hospital District of Helsinki and Uusimaa (HUS), as approved by the ethical board of the Joint Authority of the HUS, Finland (Dnro: 85/13/03/00/15). We obtained written informed consent from the patients and the studies were conducted in accordance with the Declaration of Helsinki.

Patient cohort. The Cancer Genome Atlas (TCGA) human lung adenocarcinoma (LUAD) bulk RNAseq datasets: PanCancer Atlas, TCGA (n = 566) (19), and Collisson et al. Nature, TCGA (n = 230) (1) with RSEM estimated batch normalized median expression values were downloaded from the cBioportal (https://www.cbioportal.org/). From these, *STK11*/*LKB1* mutant (*K*^{Mut};*LKB1*^{Mut} = *KL)* and *KRAS* control (*K*^{Mut};*LKB1*^{Wt} = *K)* samples were selected based on loss of function mutations in *LKB1*. Mutation data of the samples were accessed from the cBioportal (https://www.cbioportal.org/). The fold change difference in gene expression between *KL* and *K*

samples were calculated by computing Log2 ratio of the average expression values in *LKB1* mutant and *KRAS* control samples. To generate pAMPK transcriptomes, PanCancer Atlas LUAD cohort was accessed through cBioportal. Patients were queried for pAMPK (PROT: PRKAA1_PT172), as determined by reverse phase protein array (RPPA). Whole transcriptome, correlated with pAMPK, was uploaded using the *co-expression*-tool. To obtain pAMPK transcriptome specifically in *LKB1* wildtype patients, we excluded patients harboring genomic alterations in *LKB1* locus predicted to have oncogenic driver functions (query parameter DRIVER). For the Venn diagram, the overlap between *LKB1* mutations and pAMPKα patients were divided into high (Z-score ≥ 0) and low (Z-score < 0) pAMPK groups based on RPPA-values obtained through cBioportal. For the analysis of infiltration levels of different immune cells in PanCancer Atlas patients, precalculated xCell deconvolution results were uploaded from xCell web application (https://xcell.ucsf.edu/). Respective immune subpopulations were aggregated as following:

- $CD8^+$ T-cells: $CD8^+$ T-cells + $CD8^+$ naïve T-cells + $CD8^+$ Tcm + $CD8^+$ Tem.
- $CD4^+$ T-cells: $CD4^+$ T-cells + $CD4^+$ naïve T-cells + $CD4^+$ Tcm + $CD4^+$ Tem + $CD4^+$ memory T-cells.
- Denditric cells: DC + aDC + cDC + iDC + pDC
- Macrophages: Macrophages + Macrophages.M1 + Macrophages.M2
- B-cells: B-cells + Memory B-cells + Class-switched memory B-cells + naïve B-cells + Pro B-cells

Histology, immunohistochemistry. Human and murine lung samples were fixed (formalin for human samples; paraformaldehyde for murine samples), paraffin embedded, sectioned and immunohistochemistry stained as described earlier (20). The following primary antibodies were

used: TTF-1 (1:1000, ab133638, abcam), p63 (1:5000, ab124762, abcam), phospho-AMPK-alpha (1:100, #2535, Cell Signaling), phospho-ACC (1:800, #3661, Cell Signaling), LKB1 (1:500, #13031, Cell Signaling), CD8 (1:200, #98941, Cell Signaling), CD4 (1:50, #25229, Cell Signaling), CD3 (1:150, ab16669, abcam), B2M (1:1000, ab218230, abcam) and HLA Class I ABC (1:150, ab70328, abcam). Stained slides were scanned with a digital slide scanner (3D Histech Pannoramic 250 FLASH II).

RNA sequencing and data acquisition. About 10mg tumor tissue was dissected from RNAlater (Thermo Fisher Scientific, AM7020) preserved lung tumor sample, and homogenized in Lysing Matrix Tubes (MP, 6913-100) using Precellys 24 homogenizer (Bertin Instruments, P000669-PR240-A) prior to RNA extraction with RNeasy Mini Kit (QIAGEN, 74104). mRNA-seq libraries were prepared with the SureSelect Strand Specific RNA library prep kit (Agilent Technologies) after PolyA capture, and then sequenced by single-end 75 base pairs using the Illumina NextSeq 500 platform at Biomedicum Functional Genomics Unit. Sequenced reads were aligned as described previously (20). Gene-wise aligned read counts were analyzed for differential gene expression analysis using limma-voom R package (http://bioconductor.org/packages/release/bioc/html/limma.html). For immune deconvolution of mouse lung tumors, CIBERSORTx algorithm (https://cibersortx.stanford.edu/) was utilized using default parameters using counts per million (cpm)-transformed expression matrix for mouse tumor sequencing results. Custom gene sets for mouse $CD8^+$ T-cell, $CD4^+$ T-cells, dendritic cells, monocytes, macrophages and B-cells were generated using published RNA-sequencing data obtained from purified immune populations (GSE109125).

Immune Signature gene set

Human *KL* LUAD Immune Signature gene set was created by pooling unique genes from the hallmark gene sets (1383 genes in total) listed in **Supplementary Table 1**. This provided a list of 973 unique genes (**Supplementary Table 2**) which were assigned as immune signature genes. The list of immune signature genes were used as gene set to perform GSEA on fold change ranked expressed genes in mouse *KL* and *KAA* datasets. The leading edge genes from the output of this analysis in *KL* and *KAA* datasets were selected and log2 fold change values of the top 75 genes were visualized using pheatmap package in R (v3.6.2).

Western blotting analysis. Western blotting analysis was performed as described earlier (20). The primary antibodies and their dilutions were as follows: LKB1 (1:2500, ab15095, abcam), phospho-AMPKa (1:1000, #2535, CST), B2M (1:5000, ab75853, abcam), H3K27m3 (1:1000, 07-449, Merck Millipore), HLA Class I ABC (1:1000, ab70328, abcam) and GAPDH (1:15000#2118, CST). Quantification of B2M protein level was performed using Image J: B2M band sizes were normalized to that of GAPDH, and finally to corresponding empty vector controls.

Statistical analyses. Statistical analyses were performed using GraphPad Prism 7.0c. Unpaired 2-tailed student T-test or Mann Whitney test was used to determine the significance between 2 groups, and Ordinary one-way ANOVA with Tukey's multiple comparisons test was used to determine the significance among three groups. Log-rank (Mantel-Cox) test was used to determine the significance of Kaplan-Meier plot. Data are presented as mean ± standard error (s.e.m). Statistical significance was set at P-value of NS>0.05, *<0.05, **<0.01, ***<0.001, and ****<0.0001.

Data Availability Statement. RNA sequencing data is available at Gene Expression Omnibus under the accession number GSE175479.

Results

Correlation of *LKB1* mutations and attenuated AMPK activity with immune suppressive hallmarks in lung cancer patients

To interrogate how *LKB1* mutation impacts the tumor immune microenvironment (TIME), we made use of two large lung adenocarcinoma (LUAD) patient datasets (PanCancer Atlas, TCGA, 566 samples with RNASeq data from 510; Collisson et al. Nature, TCGA, 230 samples, named as Collisson dataset thereafter) (1) and compared the transcriptome between *STK11/LKB1* wildtype and mutant LUAD with *KRAS*-mutant background. We then probed for potentially relevant expression modules using Gene Expression Enrichment Analysis (GSEA) performed with the Molecular Signatures Database (MSigDB) hallmark gene set collection (**Fig. 1A and Supplementary Fig. 1A-C**). By using False Discovery Rate (FDR) < 0.05 as a cut-off, the analysis yielded 22 and 21 negatively enriched hallmark gene sets in PanCancer Atlas and Collisson datasets, respectively (**Fig. 1A and Supplementary Fig. 1A**). By ranking these hallmark gene sets according to their enrichment scores (NES values), 8 out of top 10 negative enriched hallmark gene sets are immune-related in both datasets (**Fig. 1A and Supplementary Fig. 1A**). These include 'Interferon gamma response', 'TNFα signalling' and 'IL2-STAT5 signalling' hallmarks representing genes with key roles in stimulating anti-tumor immune response and explored as targets for cancer immunotherapy (21). Taken together, these analyses demonstrated that *LKB1* mutant LUAD exhibit suppressive TIME, consistent with previous studies (5).

Given the availability of reverse phase protein array (RPPA)-derived data in subset of the PanCancer Atlas dataset (**Fig. 1C**), we sought to examine the possible association between TIME and phospho-AMPKα (pAMPKα; Thr183 in AMPKα1 and Thr172 in AMPKα2)

phosphorylated by LKB1. Consistent with the notion that LKB1 is required for AMPK activation (9), we noted that LKB1 mutations were enriched in lo-pAMPK group (76%; green) as compared to hi-pAMPK group (23%; blue) (**Fig. 1C**). We then constructed a transcriptomic profile of LUAD with low pAMPKα (lo-pAMPK) by ranking (reversed) genes with respect to their correlation coefficients between gene expression and AMPKα phosphorylation level (low to high pAMPKα). Interestingly, the GSEA analysis indicated that lo-pAMPK was also associated with a suppressive TIME as evidenced by the same hallmarks identified (**Fig. 1B**), suggesting inactivation of AMPK could mediate the suppressive TIME in *LKB1* mutant LUAD. Importantly, digital deconvolution (xCell) of RNAseq data from PanCancer Atlas (TCGA) showed decreased infiltration of $CD8^+$ and $CD4^+$ T cells in lo-pAMPK LUAD (**Supplementary Fig. 2A-B**), further demonstrating that LUAD with attenuated AMPK activity is associated with suppressed TIME.

AMPK inactivation accelerates *Kras*-driven tumorigenesis and elicits suppressive tumor immune microenvironment

To establish whether the suppressive TIME observed in LUAD patient with lo-pAMPK is causally linked with AMPK inactivation, we crossed $Kras^{LSL\text{-}G12D/+}$ mice with mice carrying $AMPK\alpha1^{fl/fl}$ and $AMPK\alpha2^{fl/fl}$ alleles or mice carrying $Lkb1^{fl/fl}$ allele as a control leading to the generation of the following genotypes: (i) $Kras^{LSL\text{-}G12D/+}$ *(K)*; (ii) $Kras^{LSL\text{-}G12D/+}$*; *$Lkb1^{fl/fl}$ (*KL*); (iii) $Kras^{LSL\text{-}G12D/+}$*;*$AMPK\alpha1^{fl/fl}$*;*$\alpha2^{fl/fl}$ (*KAA*); (iiii) $AMPK\alpha1^{fl/fl}$*;*$\alpha2^{fl/fl}$ (*AA*). Intranasal instillation of adenovirus expressing Cre-recombinase (Ad-Cre) in these mice activated KrasG12D in the lung epithelium and homozygous deletion of *Lkb1* in *KL* and *AMPKα1* and *AMPKα2* in *KAA* and *AA* mice (**Supplementary Fig. 3A**). Recombination of both *AMPKα1* and *AMPKα2* flox alleles from the dissected *KAA* tumors confirmed the deletion of *AMPKα1* and *AMPKα2*

(**Supplementary Fig. 3C**). Consistently, immunohistochemical staining (IHC) with phospho-Acetyl-CoA Carboxylase (pACC), phospho-AMPKα (p-AMPKα) and LKB1 antibodies on the serial sections from the lung tumors confirmed the reduced expression of Lkb1 in *KL* tumors and reduced pACC and pAMPK in both *KL* and *KAA* tumors (**Supplementary Fig. 3D**).

As expected (7), *KL* mice had a shortened median survival (45 days post Ad-Cre) as compared to *K* mice (170 days post Ad-Cre) (**Fig. 2A and Supplementary Fig. 3B**). Notably, *KAA* mice also had a significantly shortened survival (127 days post Ad-Cre) compared to *K* mice (**Supplementary Fig. 3B**), becoming progressively moribund with respiratory distress starting at 77 days (post Ad-Cre) as compared to 98 days of *K* mice (**Fig. 2A**). Consistently, at 90 days post Ad-Cre *KAA* lungs showed 1.8-fold increase in tumor burden compared to *K* mice (**Fig. 2B-C**). The acceleration of tumorigenesis in *KAA* mice are in line with a recent study using *in vivo* CRISPR/Cas9 mediated genome editing demonstrating that inactivation of AMPKα1 and α2 accelerate *Kras*-driven lung tumorigenesis albeit to lesser extent compared to inactivation of SIK family proteins (10). An earlier study (22) did not note accelerated tumorigenesis following AMPK which may be due to differences in background, approach or efficiency of recombination.

LKB1 loss has been shown to be associated with the appearance of tumors with squamous differentiation (7) in addition to adenocarcinomas. Based on staining with TTF-1 and p63 antibodies all tumors in the *KAA* mice represent adenocarcinomas (**Fig. 2D**), suggesting that other LKB1 substrates are involved in the squamous differentiation noted in *KL* tumors.

To investigate whether AMPKα1/α2 inactivation has an impact on the TIME, we analysed T-cell infiltration in the tumors by staining and quantification (**Fig. 2E-F and Supplementary Fig. 3E**). In the control *KL* tumors a significant reduction of total T-cells ($CD3^+$, 3.91% of total area in *K*

vs 1.49% in *KL*), cytotoxic T-cells ($CD8^+$, 0.83% of total area in *K* vs 0.54% in *KL*) as well as helper T-cells ($CD4^+$, 0.49% of total area in *K* vs 0.41% in *KL*) was noted as expected (5, 8, 23). Interestingly the *KAA* tumors also exhibited a reduction of infiltrated $CD3^+$ (3.91% of total area in *K* vs 2.10% in *KAA*), $CD8^+$ (0.83% of total area in *K* vs 0.50% in *KAA*) as well as $CD4^+$ T-cells (0.49% of total area in *K* vs 0.35% in *KAA*) indicating AMPK loss fosters a non-T-cell-inflamed TIME in *Kras*-driven LUAD similarly to Lkb1 loss.

Identification of an immune suppressive transcriptomic signature in AMPK-deficient *Kras*-driven lung adenocarcinoma

To characterize the tumor microenvironment of *KL* and *KAA* mouse tumors in greater detail, we measured global gene expression changes by RNA-seq from primary tumors micro-dissected from *K*, *KL* and *KAA* lungs. Unbiased GSEA analysis on the fold-change ranked expressed genes in *KAA* lung tumors showed strong negative enrichment of immune signature gene sets - 6 of top 10 hallmark gene sets were immune-related, including interferon and inflammatory responses similarly to *KL* tumors (**Fig. 3A**). Consistent with the TCGA LUAD study (1) as well a study of syngeneic tumor model with Lkb1 deficiency (5) , our results did not provide evidence for neutrophil enrichment as noted in one study (8). Next, we compared the *KAA* mouse model with *KL* human LUAD (*KL1*, PanCancer Atlas, TCGA; *KL2 (1)*), lo-pAMPK human LUAD (Low pAMPK; *LKB1* wildtype) as well as the *KL* LUAD mouse model by comparing GSEA hallmarks of each (**Fig. 3B and Supplementary Fig. 4A**). Remarkably, the sets enriched in *KAA* shared a striking overall similarity with *KL* and lo-pAMPK patient sets with several immune-related hallmarks. Interestingly *KAA* GSEA analysis demonstrated a higher similarity to human sets than the *KL* mouse model, which as expected (5, 8) also displayed negative enrichment of several immune-related hallmarks (**Fig. 3B**). Furthermore, deconvolution analysis using CIBERSORTx

(https://cibersortx.stanford.edu/), a computational method for quantifying cell fractions from bulk RNAseq profiles, validated the decreased infiltration of $CD8^+$ T cells in both *KL* and *KAA* as well as $CD4^+$ T cells in *KAA* LUAD (**Supplementary Fig. 4B**). Therefore, these results are in line with our IHC analysis (**Fig. 2E-F and Supplementary Fig. 3E**) and provide evidence, at the molecular level, that AMPK inactivation drives a suppressive TIME with high similarity to human *LKB1* mutant LUAD suggesting a major role for AMPK in mediating LKB1 effects on immune evasion.

To further delineate clinically relevant mechanisms and genes that could contribute to the immune evasion observed in both *KL* and *KAA* mouse LUAD, we derived an Immune Signature gene set consisting of 973 genes (**Supplementary Table 1**) by pooling unique genes from 8 immune function related hallmark gene sets (**Supplementary Table 1**) in the *KL* human LUAD datasets (see Materials and Methods, **Fig. 3B**) and performed GSEA in both *KL* and *KAA* mouse LUAD. The analysis revealed significant enrichment of the human *KL* LUAD immune signature (Immune Signature) gene set in both *KL* and *KAA* mouse LUAD, and notably the significance was much more profound in *KAA* than *KL* mouse LUAD (**Fig. 3C**). To gain further mechanistic insight into downstream pathways potentially mediating the suppressive immune signature in both *KL* and *KAA* LUAD, we performed leading edge gene analysis from the GSEA (Immune Signature) of both *KL* and *KAA* mouse LUAD (ranked by GSEA of *KAA* LUAD, **Fig. 3D**) and focused on genes intrinsic to the tumor cells. We found both *KL* and *KAA* tumors have suppressed expression of antigen processing and presentation related genes, including *Nlrc5*, *B2m* (**Fig. 3D-E and Supplementary Fig. 4C**). Notably, both *NLRC5* and *B2M* are frequently downregulated in many different cancers by enabling immune evasion (24, 25), and a recent study identified an evolutionarily conserved function of polycomb repressive complex 2 (PRC2)

in epigenetically modulating the regulation of *NLRC5* and antigen presentation pathway including *B2M* (26). Indeed, both murine (*KAA* and *KL*) and human (*KL* and lo-pAMPK) LUAD display significantly suppressed expression of PRC2 target genes (**Supplementary Fig. 4E**), corroborating with previous reports on the regulation of PRC2/EZH2 activity by either AMPK (27) or LKB1 (28). Notably, treatment of *LKB1* mutant NSCLC cells line A549 with EZH2 inhibitor GSK126 led to restoration of B2M and HLA Class Ia expression with concomitant downregulation of H3K27me3 (**Supplementary Fig. 4D**), suggesting that PRC2/EZH2 activation could be a potential mechanism to silence antigen presentation pathway and elicit the evasive TIME in *LKB1* mutant LUAD. Taken together, these analyses demonstrate that the immune signature of *KL* human LUAD is recapitulated by AMPK inactivation and therefore provide further evidence for the contribution of AMPK inactivation to the suppressive TIME in *KL* LUAD.

AMPK inactivation downregulates MHC Class I genes

Antitumor immune response depends on the recognition of tumor-specific neoantigens presented through human leukocyte antigen class I (HLA-I)-encoded major histocompatibility complex (MHC) class I molecules by cytotoxic T-cells ($CD8^+$) (29). Recently, loss of heterozygosity (LOH) at the *HLA-I* loci (30)(31) and homozygous loss of ß2-microglobulin *(B2M)* or downregulation of B2M expression (25) have been identified as a mechanism of immune evasion and resistance to immune checkpoint inhibitors (ICI) in multiple cancer types including NSCLC. We noted that B2M was significantly reduced in both *KL* and *KAA* mouse LUAD at both transcriptional level (**Fig. 3E and Supplementary Fig. 4C)** and by immunohistochemistry (**Fig. 4A and 4B**). Importantly, *B2M* was also reduced in human *KL* LUAD cohorts *(***Fig. 4C***)* and accompanied by reduction of several MHC class I genes *(HLA-B*, *HLA-C, HLA-E and HLA-F)*

*(***Supplementary Fig. 5A***)* as well as immunoproteasome related genes (*PSMB8*, *PSMB9*, *PSMB10* and *UBE2L6*) (**Supplementary Fig. 5B**) as noted by a recent study in human *KL* LUAD (32). The reduction of *B2M* expression was also noted in human lung cancer cell lines (Cancer Cell Line Encyclopedia, **Supplementary Fig. 5C**) demonstrating the reduction in a tumor cell intrinsic mechanism. To investigate the relationship between AMPK activity and B2M levels more directly, we reconstituted *LKB1* null A549 human LUAD cells ($Kras^{G12S};LKB1^{-/-}$) with a constitutively active AMPKα1 (AMPKα1-T183E). Interestingly, reconstitution of AMPKα1 activity by AMPKα1-T183E increased B2M levels significantly and comparably to reconstitution of LKB1. As expected, expression of wild-type AMPKα1 was not sufficient to reconstitute AMPK activity in cell line without LKB1 (**Fig. 4D and Supplementary Fig. 5D)**.

Reduced AMPK activity in LUAD associated with attenuated expression of antigen presentation components and immune evasion

To investigate whether low pAMPKα associated with expression of antigen presentation genes we compared the mRNA expression of *B2M* and MHC class I chain encoding genes between pAMPK high and low LUAD with wildtype *LKB1*. The results indicated that *B2M (***Fig. 5A***)* as well as all the MHC class I chain encoding genes *(HLA-A, HLA-B*, *HLA-C, HLA-E, HLA-F* and *HLA-G)* were significantly downregulated in human LUAD with reduced pAMPK (lo-pAMPK, *LKB1* wildtype, **Supplementary Fig. 6A**). Similar to the observation in mouse *KAA* and *KL* LUAD, the MHC class I transactivator *NLRC5* was downregulated in lo-pAMPK (*LKB1* wildtype, **Fig. 5B**) and *KL* human LUAD (**Supplementary Fig. 6B**). Consistent with *KL* patients (**Supplementary Fig. 5B**), we also noted suppressed expression of immunoproteasome components in *LKB1* wildtype patients with lo-pAMPK (**Supplementary Fig. 6C**). Previous

analysis of large collection of NSCLC tissue microarray samples (more than 400) revealed that the surface expression of *B2M* and *HLA class I* genes correlates with infiltration of $CD8^+$ cytotoxic T cell in the tumors (33). Thus, we compared the composition of T cells between pAMPK high (hi-pAMPK) and low (lo-pAMPK) LUAD by digital deconvolution (xCell) of RNAseq data from PanCancer Atlas (TCGA) in cases where *LKB1* mutations were not identified. Interestingly, lo-pAMPK was associated with decreased infiltration of $CD8^+$ (**Fig. 5C)** and $CD4^+$ (**Fig. 5D)** T cells, similar to LUAD with identified *LKB1* mutations as well as with *KL* and *KAA* mouse LUAD. Strikingly, the LUAD cases with low pAMPK (lo-pAMPK, **Fig. 5E**) extended significantly beyond cases with identified *LKB1* mutations suggesting that AMPK inactivation is sufficient to attenuate antigen presentation and immune evasion in human LUAD.

Discussion

Our study provides evidence that the clinically relevant immune evasion noted in *LKB1* mutant lung cancer is due to subsequent inactivation of AMPK and attenuation of antigen presentation.

The identification of AMPK as a mediator of immune evasion provides important mechanistic insight and potential target for therapeutic intervention. The observation complements the earlier reports that the LKB1 substrates MARK1 and MARK4 are required for LKB1 to suppress the EMT transcription factor Snail and metastasis (34) and that the LKB1 substrates SIK1 and SIK3 are required for growth suppression by LKB1 in lung cells (11, 35). Whether the immune evasion noted in this study following AMPK loss – and not studied by others – is causally associated with accelerated progression remains to be resolved thoroughly. Furthermore, our study (using Cre/LoxP mediated AMPK knockout) is consistent with Murray et al 2019 (using CRISPR/Cas9 mediated gene editing) (35) as we both observed increased tumor area/burden (**Fig. 2B and 2C in this study and Fig. 1D and 1F in Murray et al 2019**) albert at variable degrees, whereas Eichner et al 2019 did not observe increased tumorigenesis using either Ad-Cre or Lenti-Cre induced Cre/LoxP mediated AMPK knockout (22). While one trivial explanation might be due to the lower AdCre dose used in Eichner et al 2019 ($1x10^6$ PFU vs $5x10^7$ PFU in this study), it is notable that in both murine *KL* mice – which displays enhanced tumor growth compared to *K* mice (36) – and *LKB1* mutant NSCLC cell lines (37) as well as primary tumors (this study) both AMPK phosphorylation and AMPK dependent phosphorylation of ACC are nearly completed abrogated, suggesting that inactivation of AMPK is associated with tumor growth in *LKB1*-mutant NSCLC. Together these results suggest that LKB1 substrates mediate specific downstream effects of LKB1 contributing to tumor suppression and provides a rationale for not finding the substrates inactivated alone in human cancers.

Consistent with increasing evidence that cancer cells can evade immune surveillance by attenuating antigen presentation machinery (APM) (38), we identified reduction of several APM components including B2M, the scaffolding component of MHC-I complex, in both human and mouse *KL* LUAD, mouse *KAA* LUAD as well as in human LUAD with reduced pAMPKα (lo-pAMPK). This is consistent with the observed co-regulation of APM components (39) to meet with local requirements for an adequate immune response (39) by master regulators such as NLRC5 (39). Interestingly, *NLRC5* is downregulated in both *KL* and *KAA* mouse LUAD (**Fig. 3D-E**) as well as in human *KL* LUAD (**Supplementary Fig. 6B**) and lo-pAMPK LUAD (**Fig. 5B**), providing evidence for NLRC5 as a potential mediator for the regulation of APM genes by LKB1 via AMPK. A potential link between AMPK, NLRC5 and APM components is provided by the observations that AMPK suppresses the PRC2 histone methylase complex through phosphorylation of that PRC2 suppresses NLRC5 and APM components to enable immune evasion in multiple cancer types (26). This is consistent with our observation that also other PRC2 targets are downregulated in both human and mouse *KL* and *KAA* (lo-pAMPK) LUAD (**Supplementary Fig. 4E**) and that EZH2 inhibition led to upregulation of B2m and HLA Class Ia expression in *LKB1* mutant NSCLC cell line (**Supplementary Fig. 4D**). Taken together, these observations provide a possible mechanism for the decreased antigen presentation following defects in LKB1 whereby the resulting inactivation of AMPK enables PRC2 to suppress NLRC5 and APM components such as B2M.

The study identified attenuated phospho-AMPKα (lo-pAMPK) as a new biomarker associating with a suppressive TIME. This is interesting from a clinical point of view as: i) a suppressive TIME has been associated with resistance to PD-1 immunotherapy (6); ii) *LKB1* mutations represent the most prevalent identified mechanism of primary resistance to PD-1/PD-L1 axis

inhibitors in LUAD (5); and iii) the remarkable similarity of the TIME in *LKB1* mutant and lo-pAMPK LUAD (this study). As the landscape of primary resistance to PD-1 immunotherapy in LUAD is not fully understood and the current approaches to investigate loss of LKB1 by mutation screens (40) or LKB1 staining (2) may not be comprehensive due to e.g. non-genomic alterations (41) or defects in cofactors required for LKB1 function (42), there is a clear unmet need for new biomarkers to predict checkpoint therapy resistance.

The results here indicate lo-pAMPK represents not only a potential surrogate biomarker for LKB1 inactivation (**Fig. 5E**) but more importantly a biomarker identifying a larger LUAD set with attenuation of the pathway critical for maintenance of antigen presentation. In PanCancer Atlas patients for which both genomic and phosphorylation data was available, lo-pAMPK was noted not only in 39 patients with identified *LKB1* mutations, but importantly in 114 additional patients with a similar suppressed TIME (**Fig. 3B and Fig. 5C-D**) and reduced APM genes (**Fig. 5A-B and Supplementary Fig. 6A-B**) as those with *LKB1* mutations. This suggests that the primary resistance to PD-1 immunotherapy noted in *LKB1* mutant LUAD (5) could extend to the additional patients with lo-pAMPK but without an identified *LKB1* mutation. It will be interesting to investigate whether in the additional lo-pAMPK patients LKB1 inactivation had gone undetected (2) or whether there might be alternative ways to attenuate AMPK (43–45). However, from a clinical standpoint the discovery of lo-pAMPK identifying an enlarged set of patients with a suppressive TIME suggests that investigating the potential of lo-pAMPK in predicting primary resistance to PD-1/PD-L1 immunotherapy in LUAD patients is a priority. Based on the our initial attempt with limited amount of NSCLC patient samples, it is notable that pAMPK and B2M are both absent in *LKB1* mutant tumor (**Supplementary Fig. 6D**) prompting future efforts with extended patient samples to validate the utility of pAMPK IHC as a biomarker.

Acknowledgements

We thank Saara Ollila and Elina Niemelä for insightful discussions and Saana Ruusulampi and Melissa Montrose for technical assistance. We thank Gonghong Wei and Qin Zhang for constructive suggestions and help with LUAD patient data analysis. We thank Kaisa Salmenkivi from the Department of Radiology and Pathology at Uusimaa Hospital District (HUS) and Jere Linden from Finnish Center for Laboratory Animal Pathology for histology and pathology examination. We thank Laboratory Animal Center, Genome Biology Unit and Biomedicum Functional Genomics Unit for excellent service.

References

1. Collisson EA, Campbell JD, Brooks AN, Berger AH, Lee W, Chmielecki J, et al. Comprehensive molecular profiling of lung adenocarcinoma: The cancer genome atlas research network. Nature 2014; 511: 543-550.
2. Calles A, Sholl LM, Rodig SJ, Pelton AK, Hornick JL, Butaney M, et al. Immunohistochemical Loss of LKB1 Is a biomarker for more aggressive biology inKRAS-mutant lung Adenocarcinoma. En: *Clinical Cancer Research*. American Association for Cancer Research Inc., pp. 2851-2860.
3. Bonanno L, Paoli A De, Zulato E, Esposito G, Calabrese F, Favaretto A, et al. LKB1 Expression Correlates with Increased Survival in Patients with Advanced Non–Small Cell Lung Cancer Treated with Chemotherapy and Bevacizumab. Clin Cancer Res 2017; 23: 3316-3324.
4. Chen Z, Cheng K, Walton Z, Wang Y, Ebi H, Shimamura T, et al. A murine lung cancer co-clinical trial identifies genetic modifiers of therapeutic response. Nature 2012; 483: 613-617.
5. Skoulidis F, Goldberg ME, Greenawalt DM, Hellmann MD, Awad MM, Gainor JF, et al. STK11/LKB1 mutations and PD-1 inhibitor resistance in KRAS-mutant lung adenocarcinoma. Cancer Discov 2018; 8: 822-835.
6. Cristescu R, Mogg R, Ayers M, Albright A, Murphy E, Yearley J, et al. Pan-tumor genomic biomarkers for PD-1 checkpoint blockade-based immunotherapy. Science (80-); 362. Epub ahead of print 2018. DOI: 10.1126/science.aar3593.
7. Ji H, Ramsey MR, Hayes DN, Fan C, McNamara K, Kozlowski P, et al. LKB1 modulates lung cancer differentiation and metastasis. Nature 2007; 448: 807-810.
8. Koyama S, Akbay EA, Li YY, Aref AR, Skoulidis F, Herter-Sprie GS, et al. STK11/LKB1 deficiency promotes neutrophil recruitment and proinflammatory cytokine production to suppress T-cell activity in the lung tumor microenvironment. Cancer Res 2016; 76: 999-1008.
9. Shackelford DB, Shaw RJ. The LKB1-AMPK pathway: metabolism and growth control in tumour suppression. Nat Rev Cancer 2009; 9: 563-575.

10. Murray CW, Brady JJ, Tsai MK, Li C, Winters IP, Tang R, et al. An LKB1-SIK Axis Suppresses Lung Tumor Growth and Controls Differentiation. Cancer Discov 2019; 9: 1590-605.
11. Hollstein PE, Eichner LJ, Brun SN, Kamireddy A, Svensson RU, Vera LI, et al. The AMPK-Related Kinases SIK1 and SIK3 Mediate Key Tumor-Suppressive Effects of LKB1 in NSCLC. Cancer Discov 2019; 9: 1606-1633.
12. Zhang Z, Li F, Tian Y, Cao L, Gao Q, Zhang C, et al. Metformin Enhances the Antitumor Activity of CD8 + T Lymphocytes via the AMPK–miR-107–Eomes–PD-1 Pathway. J Immunol 2020; 204: 2575-2588.
13. Wang S, Lin Y, Xiong X, Wang L, Guo Y, Chen Y, et al. Low-Dose Metformin Reprograms the Tumor Immune Microenvironment in Human Esophageal Cancer: Results of a Phase II Clinical Trial. Clin Cancer Res 2020; 26: 4921-4932.
14. Saito A, Kitayama J, Horie H, Koinuma K, Ohzawa H, Yamaguchi H, et al. Metformin changes the immune microenvironment of colorectal cancer in patients with type 2 diabetes mellitus. Cancer Sci 2020; 111: 4012-4020.
15. Zhou G, Myers R, Li Y, Chen Y, Shen X, Fenyk-Melody J, et al. Role of AMP-activated protein kinase in mechanism of metformin action. J Clin Invest 2001; 108: 1167-1174.
16. Jackson EL, Willis N, Mercer K, Bronson RT, Crowley D, Montoya R, et al. Analysis of lung tumor initiation and progression using conditional expression of oncogenic K-ras. Genes Dev 2001; 15: 3243-3248.
17. Bardeesy N, Sinha M, Hezel AF, Signoretti S, Hathaway NA, Sharpless NE, et al. Loss of the Lkb1 tumour suppressor provokes intestinal polyposis but resistance to transformation. Nature 2002; 419: 162-167.
18. DuPage M, Dooley AL, Jacks T. Conditional mouse lung cancer models using adenoviral or lentiviral delivery of Cre recombinase. Nat Protoc 2009; 4: 1064-1072.
19. Liu J, Lichtenberg T, Hoadley KA, Poisson LM, Lazar AJ, Cherniack AD, et al. An Integrated TCGA Pan-Cancer Clinical Data Resource to Drive High-Quality Survival Outcome Analytics.

Cell 2018; 173: 400-416.e11.

20. Gao Y, Yan Y, Tripathi S, Pentinmikko N, Amaral A, Päivinen P, et al. LKB1 Represses ATOH1 via PDK4 and Energy Metabolism and Regulates Intestinal Stem Cell Fate. Gastroenterology 2020; 158: 1389-1401.e10.

21. Berraondo P, Sanmamed MF, Ochoa MC, Etxeberria I, Aznar MA, Pérez-Gracia JL, et al. Cytokines in clinical cancer immunotherapy. Br J Cancer 2019; 120: 6-15.

22. Eichner LJ, Brun SN, Ross DS, Shaw RJ, Svensson RU. Genetic Analysis Reveals AMPK Is Required to Support Tumor Growth in Murine Kras-Dependent Lung Cancer Models. Cell Metab 2019; 29: 285-302.

23. Biton J, Mansuet-Lupo A, Pécuchet N, Alifano M, Ouakrim H, Arrondeau J, et al. TP53, STK11, and EGFR mutations predict tumor immune profile and the response to anti–PD-1 in lung adenocarcinoma. Clin Cancer Res 2018; 24: 5710-5723.

24. Yoshihama S, Vijayan S, Sidiq T, Kobayashi KS. NLRC5/CITA: A Key Player in Cancer Immune Surveillance. Trends in Cancer 2017; 3: 28-38.

25. Gettinger S, Choi J, Hastings K, Truini A, Datar I, Sowell R, et al. Impaired HLA class I antigen processing and presentation as a mechanism of acquired resistance to immune checkpoint inhibitors in lung cancer. Cancer Discov 2017; 7: 1420-1435.

26. Burr ML, Sparbier CE, Chan KL, Chan YC, Kersbergen A, Lam EYN, et al. An Evolutionarily Conserved Function of Polycomb Silences the MHC Class I Antigen Presentation Pathway and Enables Immune Evasion in Cancer. Cancer Cell 2019; 36: 385-401.e8.

27. Wan L, Xu K, Wei Y, Zhang J, Han T, Fry C, et al. Phosphorylation of EZH2 by AMPK Suppresses PRC2 Methyltransferase Activity and Oncogenic Function. Mol Cell 2018; 69: 279-291.e5.

28. Kitajima S, Ivanova E, Guo S, Yoshida R, Campisi M, Sundararaman SK, et al. Suppression of STING Associated with LKB1 Loss in KRAS-Driven Lung Cancer. Cancer Discov 2019; 9: 34-45.

29. Dhatchinamoorthy K, Colbert JD, Rock KL. Cancer Immune Evasion Through Loss of MHC

Class I Antigen Presentation. Front Immunol 2021; 12: 636568.

30. Montesion M, Murugesan K, Jin DX, Sharaf R, Sanchez N, Guria A, et al. Somatic HLA Class I Loss Is a Widespread Mechanism of Immune Evasion Which Refines the Use of Tumor Mutational Burden as a Biomarker of Checkpoint Inhibitor Response. Cancer Discov 2021; 11: 282-292.

31. McGranahan N, Rosenthal R, Hiley CT, Rowan AJ, Watkins TBK, Wilson GA, et al. Allele-Specific HLA Loss and Immune Escape in Lung Cancer Evolution. Cell 2017; 171: 1259-1271.e11.

32. Deng J, Thennavan A, Dolgalev I, Chen T, Li J, Marzio A, et al. ULK1 inhibition overcomes compromised antigen presentation and restores antitumor immunity in LKB1-mutant lung cancer. Nat Cancer 2021; 2: 503-514.

33. Pereira C, Gimenez-Xavier P, Pros E, Pajares MJ, Moro M, Gomez A, et al. Genomic Profiling of Patient-Derived Xenografts for Lung Cancer Identifies B2M Inactivation Impairing Immunorecognition. Clin Cancer Res 2017; 23: 3203-3213.

34. Goodwin JM, Svensson RU, Lou HJ, Winslow MM, Turk BE, Shaw RJ. An AMPK-independent signaling pathway downstream of the LKB1 tumor suppressor controls snail1 and metastatic potential. Mol Cell 2014; 55: 436-450.

35. Murray CW, Brady JJ, Tsai MK, Li C, Winters IP, Tang R, et al. An lkb1–sik axis suppresses lung tumor growth and controls differentiation. Cancer Discov 2019; 9: 1590-1605.

36. Ji H, Ramsey MR, Hayes DN, Fan C, McNamara K, Kozlowski P, et al. LKB1 modulates lung cancer differentiation and metastasis. Nature 2007; 448: 807-10.

37. Carretero J, Medina PP, Blanco R, Smit L, Tang M, Roncador G, et al. Dysfunctional AMPK activity, signalling through mTOR and survival in response to energetic stress in LKB1-deficient lung cancer. Oncogene 2007 2611 2006; 26: 1616-1625.

38. Shukla A, Cloutier M, Santharam MA, Ramanathan S, Ilangumaran S. The mhc class-i transactivator nlrc5: Implications to cancer immunology and potential applications to cancer

immunotherapy. Int J Mol Sci 2021; 22: 1-36.

39. Dhatchinamoorthy K, Colbert JD, Rock KL. Cancer Immune Evasion Through Loss of MHC Class I Antigen Presentation. Front Immunol 2021; 12: 636568.

40. Sanchez-Cespedes M. A role for LKB1 gene in human cancer beyond the Peutz-Jeghers syndrome. Oncogene 2007; 26: 7825-7832.

41. Sanchez-Cespedes M, Parrella P, Esteller M, Nomoto S, Trink B, Engles JM, et al. Inactivation of LKB1/STK11 Is a Common Event in Adenocarcinomas of the Lung. Cancer Res; 62.

42. Kullmann L, Krahn MP. Controlling the master - Upstream regulation of the tumor suppressor LKB1. Oncogene 2018; 37: 3045-3057.

43. Yan Y, Ollila S, Wong IPL, Vallenius T, Palvimo JJ, Vaahtomeri K, et al. SUMOylation of AMPKα1 by PIAS4 specifically regulates mTORC1 signalling. Nat Commun 2015; 6: 1-12.

44. Suzuki T, Bridges D, Nakada D, Skiniotis G, Morrison SJ, Lin JD, et al. Inhibition of AMPK catabolic action by GSK3. Mol Cell 2013; 50: 407-419.

45. Budanov A V., Karin M. p53 Target Genes Sestrin1 and Sestrin2 Connect Genotoxic Stress and mTOR Signaling. Cell 2008; 134: 451-460.

Figure Legends

Fig. 1. Transcriptomic immune signatures suppressed in lung adenocarcinoma patients with either *LKB1* mutations or with attenuated phospho-AMPKα.

A. Negatively enriched Molecular Signatures Database (MSigDB) hallmark gene sets in *LKB1* mutant lung adenocarcinoma **(**LUAD) patients with identified *LKB1* inactivating mutations compared to controls (*KRAS* mutant in both sets) in PanCancer Atlas (TCGA) as analysed by gene set enrichment analysis (GSEA) and ranked by normalized enrichment scores (NES). Immune-related hallmarks are shown in red. NES in sets with a false discovery rate (FDR) < 0.05 are in red.

B. GSEA analysis as in **A** showing negatively enriched hallmarks in LUAD samples with low phospho-AMPKα (lo-pAMPK; including both *LKB1* wild-type and mutant samples, see **Fig. 1C** and Materials and Methods) as a biomarker for AMPK activity.

C. Oncoprint depicting the percentage of human lung adenocarcinomas (510 samples, PanCancer Atlas, TCGA) that have been profiled with RPPA (Reverse Phase Protein Arrays) into either hi-pAMPK (**in blue**) or lo-pAMPK (**in green**), and that harbour distinct genomic alterations of *LKB1* and *KRAS*.

Fig. 2. Deletion of AMPKα1 and AMPKα2 accelerates *Kras*-driven lung adenocarcinoma and elicits a suppressive tumor immune microenvironment.

A. Kaplan-Meier curve of $Kras^{LSL\text{-}G12D/+}$ (termed *K*; n=27), $Kras^{LSL\text{-}G12D/+};Lkb1^{fl/fl}$ (termed *KL*; n=27), $Kras^{LSL\text{-}G12D/+};AMPK\alpha1^{fl/fl};AMPK\alpha2^{fl/fl}$ (termed *KAA*; n=25) and $AMPK\alpha1^{fl/fl};AMPK\alpha2^{fl/fl}$ (termed *AA*; n=12) mice after inhalation with $5x10^7$ PFU of Ad-CRE. Log-rank (Mantel-Cox) test was used to determine significance: **** P<0.0001 for *K* vs *KAA*; **** P<0.0001 for *K* vs *KL*; **** P<0.0001 for *KL* vs *KAA*.

B. Representative micrographs of hematoxylin and eosin (H&E) stained left lobes of *K* and *KAA* mice 90 days post-inhalation demonstrating increased tumors burden.

C. Quantification of tumor burden (total tumor area/total lung area) in both *K* (n=7) and *KAA* (n=7) mice 90 days post-inhalation. Unpaired *t* test (two-tailed) was used to determine the significance (*P < 0.05; ** P < 0.01; *** P < 0.001).

D. H&E, TTF-1 or p63 staining of lung serial sections from *K*, *KL* or *KAA* mice with tumors classified as adenocarcinoma (ADC) or squamous cell carcinoma (SCC).

E. CD8 or CD4 immunohistochemical staining of *K*, *KL* and *KAA* lung tumor sections.

F. Quantification of $CD8^+$ and $CD4^+$ cells in tumors from indicated mouse strains as determined by percentage of marker positive surface area in IHC stained lung tumors. Each dot represents a single tumor and multiple tumors were quantified from each genotype. The largest tumor containing lobe from each mouse was selected for quantification. Minimum 4 mice per genotype were used for quantification. Number of tumors quantified for $CD8^+$ T cells: *K*, n=20; *KL*, n=14; *KAA*, n=75. Number of tumors quantified for $CD4^+$ T cells quantification: *K*, n=28; *KL*, n=16; *KAA*, n=49. Unpaired *t* test (two-tailed) was used to determine the significance (*P < 0.05; ** P < 0.01; *** P < 0.001).

Fig. 3. Identifying immune suppressive transcriptomic signatures in LUAD with attenuated AMPK

A. MSigDB Hallmark gene sets associated with AMPKα deficient *Kras*-driven LUAD (*KAA* vs *K*) as determined by GSEA and ranked by NES. The immune related hallmarks are shown in red. Hallmarks with false discovery rate (FDR) < 0.05 are shown.

B. Dot plot illustrating cross-species GSEA enrichment scores for MSigDB Hallmark gene sets from *KL* human LUAD (*KL1*, PanCancer Atlas, TCGA; *KL2*, Collisson et al. Nature 2014, TCGA), *LKB1* wildtype human LUAD with reduced pAMPK (lo-pAMPK) as well as *KL* and *KAA* mouse LUAD. NES is indicated by color and FDR in indicated by dot size. The plot is ranked by NES of *KL1* and immune-related hallmarks are highlighted in red.

C. GSEA enrichment plots representing negative enrichment of Human *KL* LUAD immune signature (Immune Signature; see material and methods) in *KAA* and *KL* tumors.

D. Leading edge gene analysis showing top 75 negatively enriched Immune Signature genes as a heatmap of fold changes in *KL* and *KAA* lung tumors ranked by GSEA of *KAA* LUAD and with antigen presentation/immunoproteasome related genes highlighted in red. The colour bars on top show the correlation between colour and log fold-change of the indicated genes.

E. Relative mRNA level of *B2m*, *Nlrc5*, *H2-K1*, *H2-D1* and *H2-T23* from mouse primary tumors micro dissected from *K*, *KL* or *KAA* lungs as assessed by quantitative real-time polymerase chain reaction (qRT-PCR) analysis. 3 tumors from each genotype were used for analysis. Unpaired *t* test (two-tailed) was used to determine the significance (*P < 0.05; ** P < 0.01; *** P < 0.001).

Fig. 4. Attenuation of the MHC Class I component ß2-microglobulin following defects in LKB1 or AMPK in lung cancer.

A. Representative IHC staining of B2m in *K*, *KL* and *KAA* lung tumors. Scale bar: 100µm.

B. Quantification of $B2M^+$ cells in tumors from indicated mouse strains as determined by percentage of marker positive surface area in IHC stained lung tumors. Each dot

represents each tumor and multiple tumors were quantified from each genotype. The largest tumor containing lobe from each mouse was selected for quantification. Minimum 4 mice per genotype were used for quantification. Number of tumors quantified for $B2m^+$ cells: *K*, n=199; *KL*, n=84; *KAA*, n=173. Unpaired t test (two-tailed) was used to determine the significance (*P < 0.05; ** P < 0.01; *** P < 0.001).

C. Dot plot graph showing RNA-sequencing by expectation maximization (RSEM) of *B2M* mRNA expression values in *K* (*KRAS* mutant and *LKB1* wildtype) or *KL* (K*RAS* mutant and *LKB1* mutant) LUAD in PanCancer Atlas (TCGA) or Collisson et al. Nature 2014 (TCGA). Number of samples in PanCancer Atlas: *K*, n=128; *KL*, n=38. Number of samples in Collisson et al. Nature 2014: *K*, n=62; *KL*, n=20. Mann Whitney test was used to determine the significance (*P < 0.05; ** P < 0.01; *** P < 0.001).

D. Western blotting analysis of cell lysates from A549 cells stably transduced with a control lentiviral vector (Control) or lentiviral constructs expressing indicated cDNAs shown on the top using antibodies indicated on the left. LKB1-K78M: kinase-deficient LKB1; LKB1-WT: wild-type LKB1; AMPKα1-WT: wild-type AMPKα1; AMPKα1-T183E: constitutively active AMPKα1.

Fig. 5. Attenuated pAMPK as a new biomarker identifying an extended set of LUAD patients with defective antigen presentation and immune evasion.

A. Dot plot showing *B2M* mRNA expression values (by RSEM) in high (hi) or low (lo) pAMPK (*LKB1* wildtype) LUAD patients (top and bottom 15^{th} percentiles respectively) from the PanCancer Atlas (TCGA). Number of samples: hi-pAMPK, n=46; hi-pAMPK, n=46. Mann Whitney test was used to determine the significance (*P < 0.05; ** P < 0.01; *** P < 0.001).

B. Comparison of NLRC5 in hi or lo-pAMPK LUAD analysed as in **A.** Number of samples: hi-pAMPK, n=46; hi-pAMPK, n=46.

C. Dot plot graph showing $CD8^+$ T-cells deconvolution scores, as determined by digital deconvolution (xCell), in hi or lo-pAMPK LUAD (*LKB1* wildtype) patients (top and bottom 15^{th} percentiles respectively) in PanCancer Atlas (TCGA). Number of samples: hi-pAMPK, n=46; hi-pAMPK, n=46.

D. Dot plot graph showing $CD4^+$ T-cells infiltration levels, determined as in **D**. Number of samples: hi-pAMPK, n=46; hi-pAMPK, n=46. Mann Whitney test was used to determine the significance from **A-D** (*P < 0.05; ** P < 0.01; *** P < 0.001).

E. **Left**: Levels of pAMPK assayed by Reverse Phase Protein Arrays (RPPA) in patients binned to hi-pAMPK (n=188; *LKB1* wildtype) and lo-pAMPK (n=114; *LKB1* wildtype) compared to *LKB1* mutant LUAD patients (n=51). Ordinary one-way ANOVA with Tukey's multiple comparisons test was used to determine the significance among the three groups. (*P < 0.05; ** P < 0.01; *** P < 0.001; **** P < 0.001). **Right**: Venn diagram illustrating the overlap of LUAD patients with hi-pAMPK (blue; 200 patients) and lo-pAMPK (green; 153 patients), where phospho-AMPKα was determined by RPPA, with LUAD patients with identified *LKB1* mutations (red, 51 patients).

Figure 1

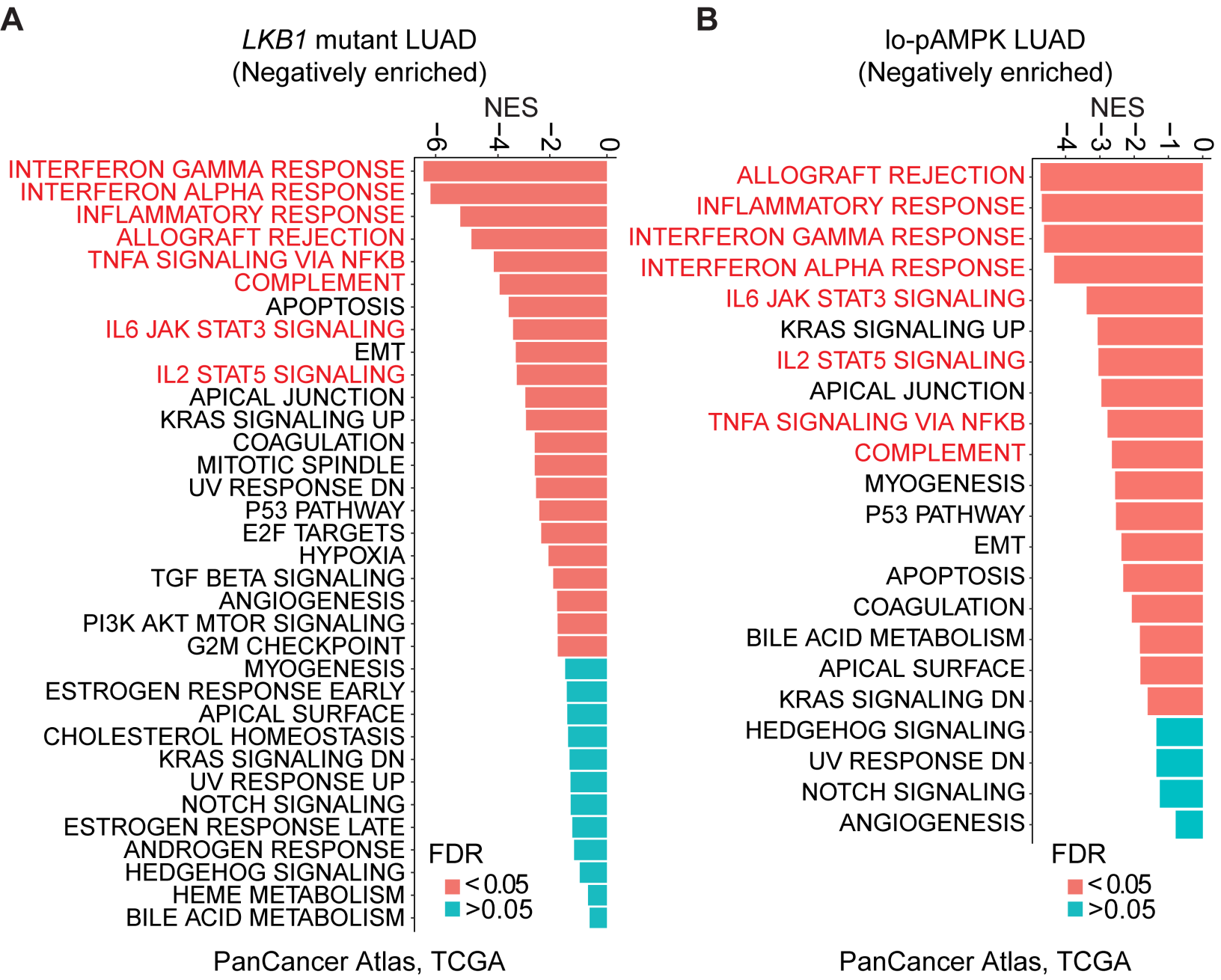
A
LKB1 mutant LUAD
(Negatively enriched)
NES
−6
−4
−2
0
INTERFERON GAMMA RESPONSE
INTERFERON ALPHA RESPONSE
INFLAMMATORY RESPONSE
ALLOGRAFT REJECTION
TNFA SIGNALING VIA NFKB
COMPLEMENT
APOPTOSIS
IL6 JAK STAT3 SIGNALING
EMT
IL2 STAT5 SIGNALING
APICAL JUNCTION
KRAS SIGNALING UP
COAGULATION
MITOTIC SPINDLE
UV RESPONSE DN
P53 PATHWAY
E2F TARGETS
HYPOXIA
TGF BETA SIGNALING
ANGIOGENESIS
PI3K AKT MTOR SIGNALING
G2M CHECKPOINT
MYOGENESIS
ESTROGEN RESPONSE EARLY
APICAL SURFACE
CHOLESTEROL HOMEOSTASIS
KRAS SIGNALING DN
UV RESPONSE UP
NOTCH SIGNALING
ESTROGEN RESPONSE LATE
ANDROGEN RESPONSE
HEDGEHOG SIGNALING
HEME METABOLISM
BILE ACID METABOLISM
FDR
< 0.05
>0.05
PanCancer Atlas, TCGA
B
lo-pAMPK LUAD
(Negatively enriched)
NES
−4
−3
−2
−1
0
ALLOGRAFT REJECTION
INFLAMMATORY RESPONSE
INTERFERON GAMMA RESPONSE
INTERFERON ALPHA RESPONSE
IL6 JAK STAT3 SIGNALING
KRAS SIGNALING UP
IL2 STAT5 SIGNALING
APICAL JUNCTION
TNFA SIGNALING VIA NFKB
COMPLEMENT
MYOGENESIS
P53 PATHWAY
EMT
APOPTOSIS
COAGULATION
BILE ACID METABOLISM
APICAL SURFACE
KRAS SIGNALING DN
HEDGEHOG SIGNALING
UV RESPONSE DN
NOTCH SIGNALING
ANGIOGENESIS
FDR
< 0.05
>0.05
PanCancer Atlas, TCGA

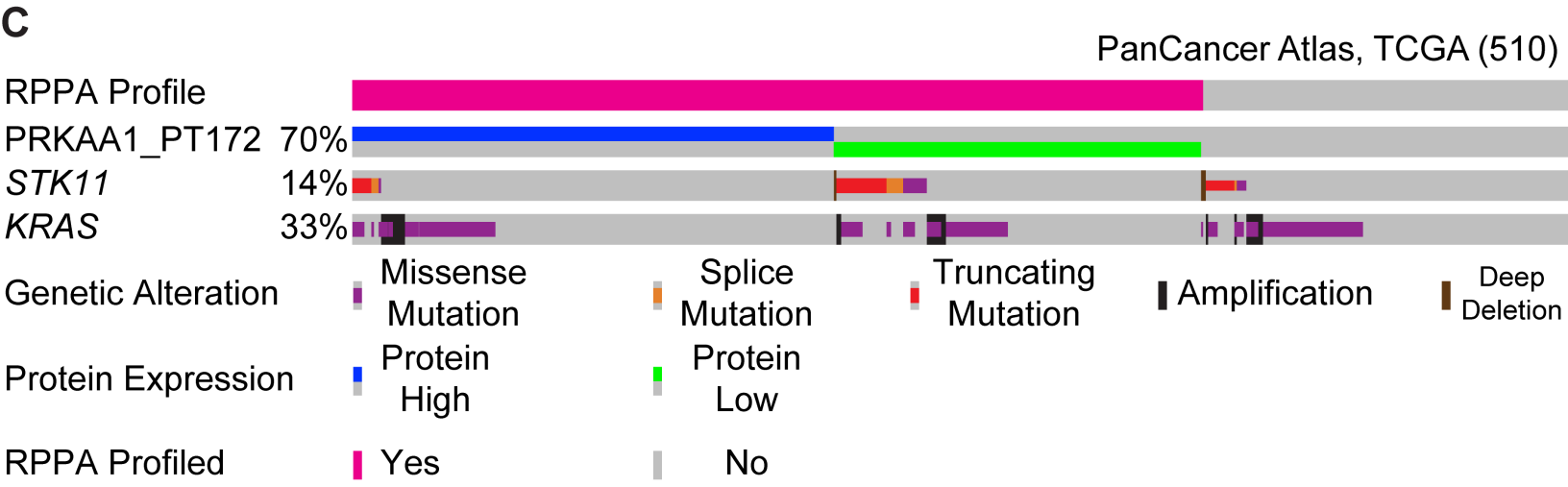
C
PanCancer Atlas, TCGA (510)
RPPA Profile
PRKAA1_PT172 70%
STK11 14%
KRAS 33%
Genetic Alteration
Missense Mutation
Splice Mutation
Truncating Mutation
Amplification
Deep Deletion
Protein Expression
Protein High
Protein Low
RPPA Profiled
Yes
No

Figure 2

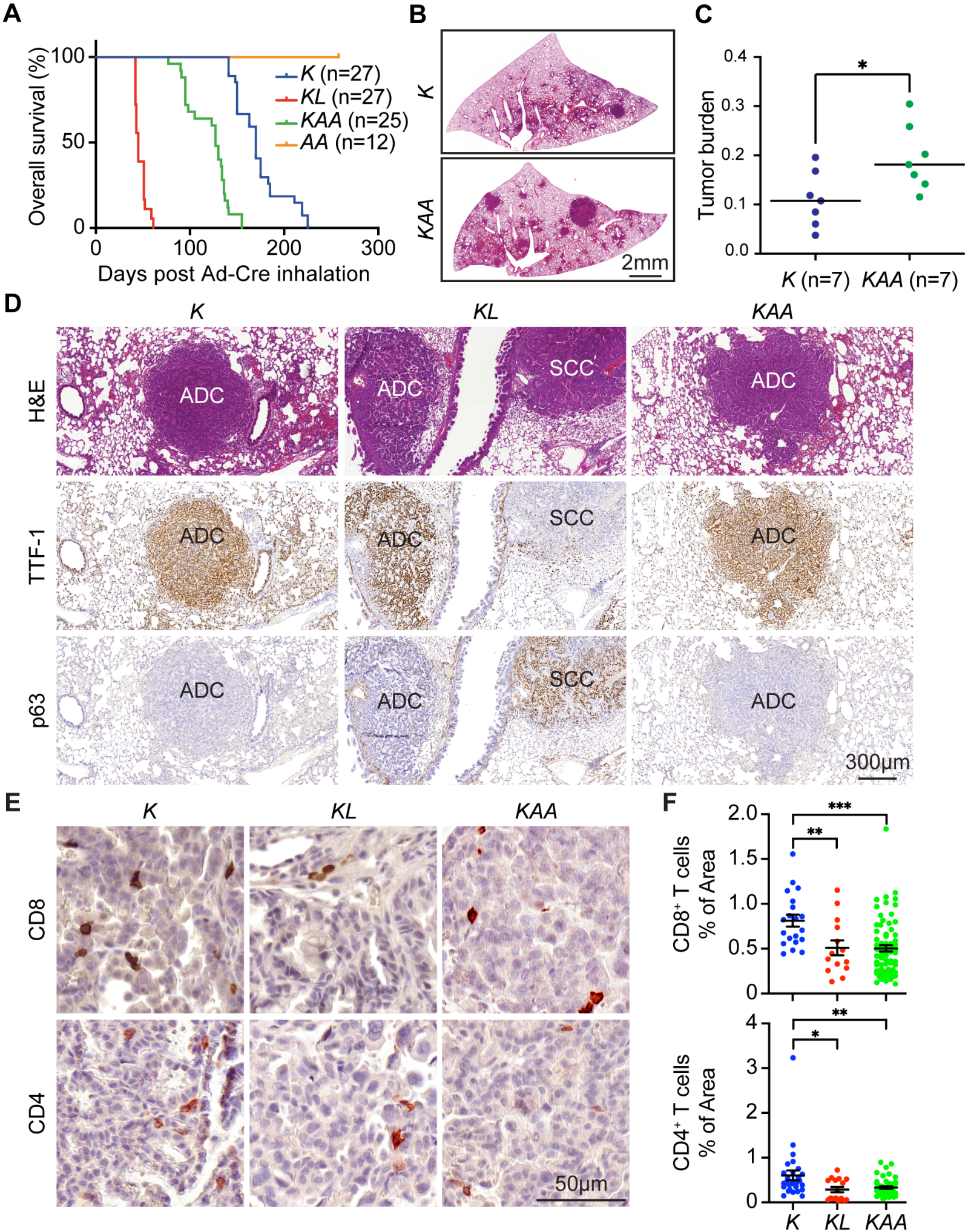
A
Overall survival (%)
100
50
0
0
100
200
300
Days post Ad-Cre inhalation
K (n=27)
KL (n=27)
KAA (n=25)
AA (n=12)
B
K
KAA
2mm
C
Tumor burden
0.4
0.3
0.2
0.1
0.0
*
K (n=7)
KAA (n=7)
D
K
KL
KAA
H&E
TTF-1
p63
ADC
SCC
300μm
E
K
KL
KAA
CD8
CD4
50μm
F
CD8+ T cells % of Area
2.0
1.5
1.0
0.5
0
***
**
CD4+ T cells % of Area
4
3
2
1
0
**
*
K
KL
KAA

Figure 3

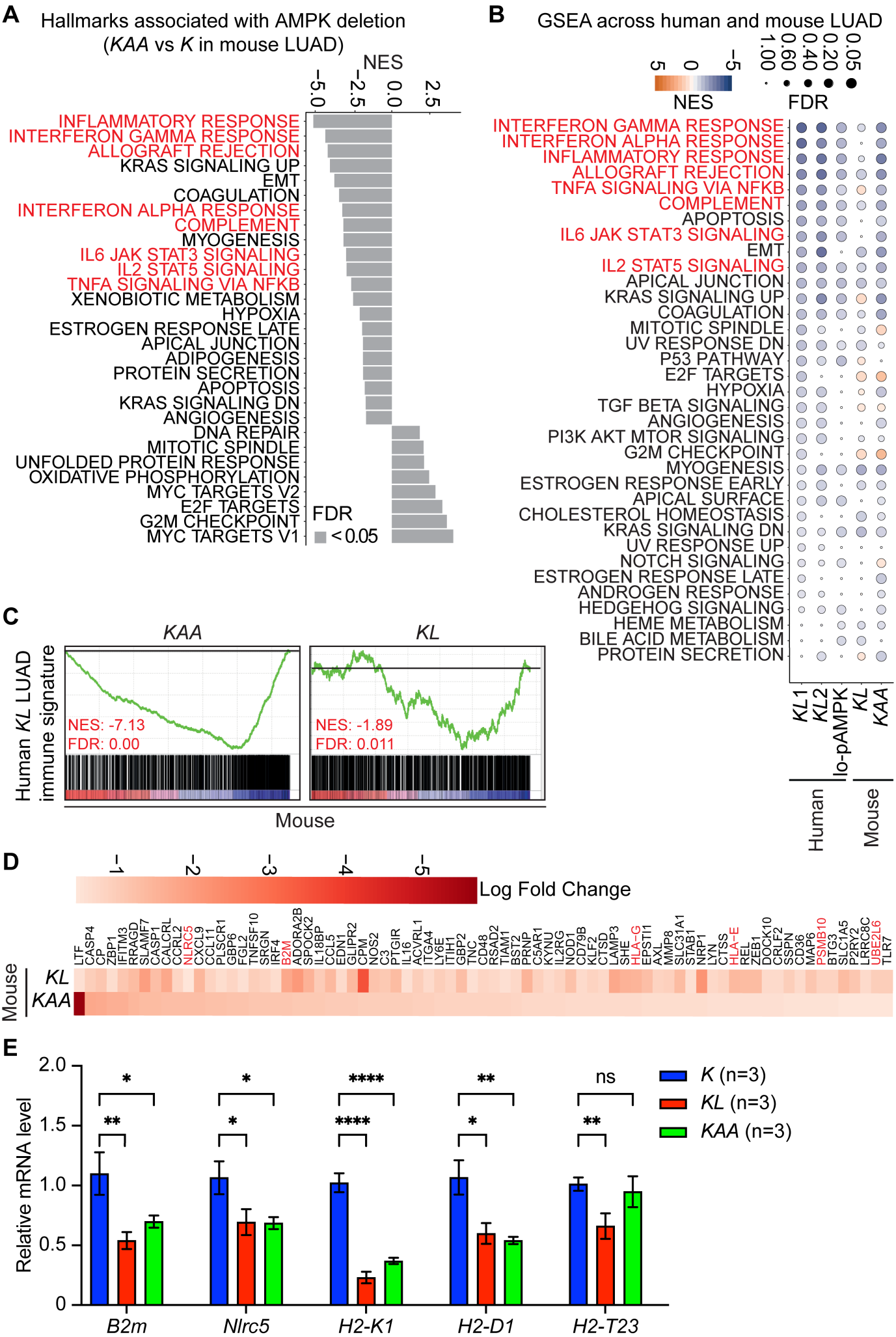
A
Hallmarks associated with AMPK deletion
(KAA vs K in mouse LUAD)
NES
−5.0
−2.5
0.0
2.5
INFLAMMATORY RESPONSE
INTERFERON GAMMA RESPONSE
ALLOGRAFT REJECTION
KRAS SIGNALING UP
EMT
COAGULATION
INTERFERON ALPHA RESPONSE
COMPLEMENT
MYOGENESIS
IL6 JAK STAT3 SIGNALING
IL2 STAT5 SIGNALING
TNFA SIGNALING VIA NFKB
XENOBIOTIC METABOLISM
HYPOXIA
ESTROGEN RESPONSE LATE
APICAL JUNCTION
ADIPOGENESIS
PROTEIN SECRETION
APOPTOSIS
KRAS SIGNALING DN
ANGIOGENESIS
DNA REPAIR
MITOTIC SPINDLE
UNFOLDED PROTEIN RESPONSE
OXIDATIVE PHOSPHORYLATION
MYC TARGETS V2
E2F TARGETS
G2M CHECKPOINT
MYC TARGETS V1
FDR
< 0.05
B
GSEA across human and mouse LUAD
5
0
−5
NES
1.00
0.60
0.40
0.20
0.05
FDR
INTERFERON GAMMA RESPONSE
INTERFERON ALPHA RESPONSE
INFLAMMATORY RESPONSE
ALLOGRAFT REJECTION
TNFA SIGNALING VIA NFKB
COMPLEMENT
APOPTOSIS
IL6 JAK STAT3 SIGNALING
EMT
IL2 STAT5 SIGNALING
APICAL JUNCTION
KRAS SIGNALING UP
COAGULATION
MITOTIC SPINDLE
UV RESPONSE DN
P53 PATHWAY
E2F TARGETS
HYPOXIA
TGF BETA SIGNALING
ANGIOGENESIS
PI3K AKT MTOR SIGNALING
G2M CHECKPOINT
MYOGENESIS
ESTROGEN RESPONSE EARLY
APICAL SURFACE
CHOLESTEROL HOMEOSTASIS
KRAS SIGNALING DN
UV RESPONSE UP
NOTCH SIGNALING
ESTROGEN RESPONSE LATE
ANDROGEN RESPONSE
HEDGEHOG SIGNALING
HEME METABOLISM
BILE ACID METABOLISM
PROTEIN SECRETION
KL1
KL2
lo-pAMPK
KL
KAA
Human
Mouse
C
KAA
KL
Human KL LUAD immune signature
NES: -7.13
FDR: 0.00
NES: -1.89
FDR: 0.011
Mouse
D
−1
−2
−3
−4
−5
Log Fold Change
LTF CASP4 CP ZBP1 IFITM3 RRAGD SLAMF7 CASP1 CALCRL CCRL2 NLRC5 CXCL9 CCL11 PLSCR1 GBP6 FGL2 TNFSF10 SRGN IRF4 B2M ADORA2B SPOCK2 IL18BP CCL5 EDN1 GLIPR2 CPM NOS2 C3 PTGIR IL16 ACVRL1 ITGA4 LY6E ITIH1 GBP2 TNC CD48 RSAD2 TIAM1 BST2 PRNP C5AR1 KYNU IL2RG NOD1 CD79B KLF2 CTSD LAMP3 SHE HLA-G EPSTI1 AXL MMP8 SLC31A1 STAB1 NRP1 LYN CTSS HLA-E REL ZEB1 DOCK10 CRLF2 SSPN CD36 MAP6 PSMB10 BTG3 SLC1A5 P2RY2 LRRC8C UBE2L6 TLR7
Mouse
KL
KAA
E
Relative mRNA level
2.0
1.5
1.0
0.5
0
*
**
*
*
****
****
**
*
ns
**
K (n=3)
KL (n=3)
KAA (n=3)
B2m
Nlrc5
H2-K1
H2-D1
H2-T23

Figure 4

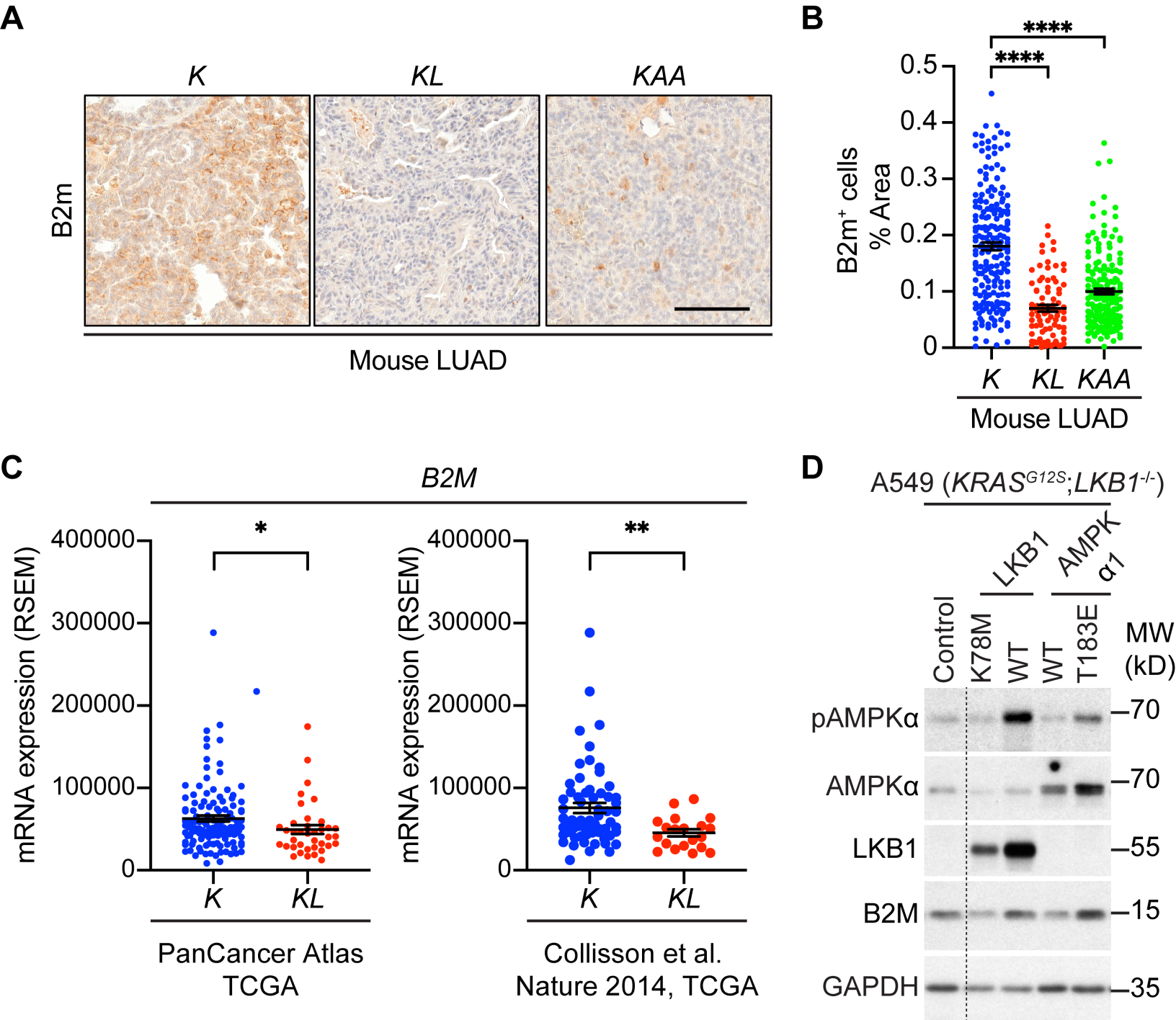
A
K
KL
KAA
B2m
Mouse LUAD
B
****
****
B2m+ cells
% Area
0.5
0.4
0.3
0.2
0.1
0
K
KL
KAA
Mouse LUAD
C
B2M
*
**
mRNA expression (RSEM)
400000
300000
200000
100000
0
K
KL
PanCancer Atlas
TCGA
Collisson et al.
Nature 2014, TCGA
D
A549 (KRASG12S;LKB1-/-)
LKB1
AMPK α1
Control
K78M
WT
WT
T183E
MW (kD)
pAMPKα
AMPKα
LKB1
B2M
GAPDH
70
70
55
15
35

Figure 5

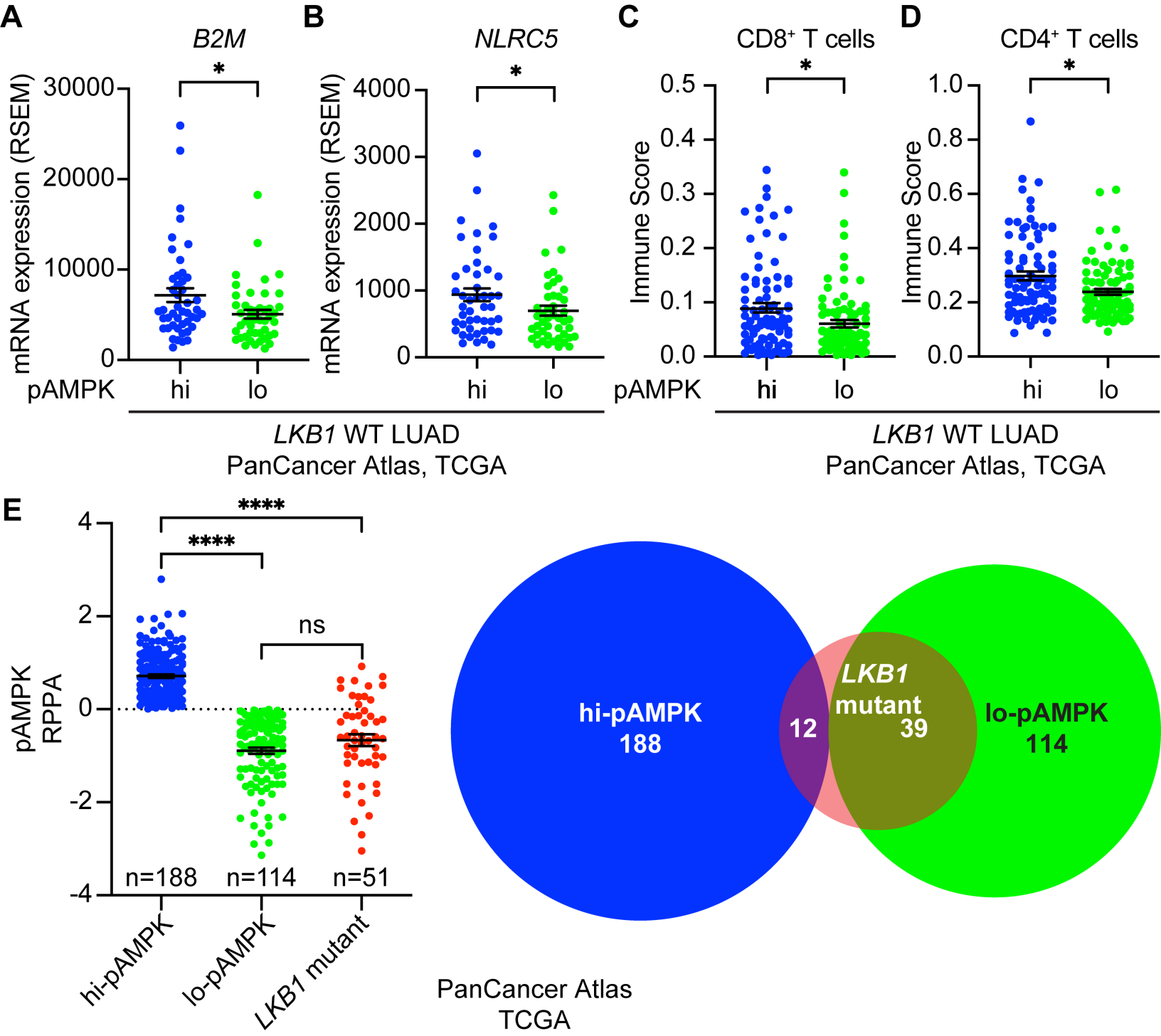
A
B2M
mRNA expression (RSEM)
30000
20000
10000
0
*
pAMPK
hi
lo
B
NLRC5
mRNA expression (RSEM)
4000
3000
2000
1000
0
*
hi
lo
LKB1 WT LUAD
PanCancer Atlas, TCGA
C
CD8+ T cells
Immune Score
0.5
0.4
0.3
0.2
0.1
0.0
*
pAMPK
hi
lo
D
CD4+ T cells
Immune Score
1.0
0.8
0.6
0.4
0.2
0.0
*
hi
lo
LKB1 WT LUAD
PanCancer Atlas, TCGA
E
pAMPK RPPA
4
2
0
-2
-4
****
****
ns
n=188
n=114
n=51
hi-pAMPK
lo-pAMPK
LKB1 mutant
PanCancer Atlas
TCGA
hi-pAMPK
188
12
LKB1
mutant
39
lo-pAMPK
114

Supplementary Materials and Methods

Image quantification. To quantitate lung tumor size, individual tumor areas and total lung areas were measured from H&E stained sections using ImageJ and the percentage of tumor area was normalized to total lung area. To quantitate immune cell infiltration level, tumors were annotated using CaseViewer software (3DHISTECH). Only tumors negative for phospho-ACC staining from *KL* and *KAA* mice were included in the analysis. For *KL*, squamous tumors were excluded from quantification. Annotations were analyzed using QuantCenter software (HistoQuant, 3DHISTECH) by recording the fraction of DAB-positive surface area. The largest tumor containing lobe from each mouse was selected for quantification and minimum 4 mice per genotype were quantified.

Plasmids. For lentiviral expression, lentiviral vector (pLenti6/V5) expressing human *LKB1* (wildtype), *LKB1*-K78M (kinase dead mutant), *AMPKα1* (wildtype) and *AMPKα1*-T183E (mutant) were generated.

Cell culture, lentiviral production and transduction. *KAA* mouse embryonic fibroblast cells (MEFs) were generated using a method described earlier (2). Adenoviral infection was performed as previously described (3). A549 and HEK293FT cell were purchased from ATCC in 1996 and regularly checked for mycoplasma contamination (monthly, LookOut@Mycoplasma PCR Detection Kit, MP0035, Sigma) during the course this study. Cells were not authenticated and all cell lines were used for experiments within 5 passages after thawing. For EZH2 inhibition experiment, A549 cells were treated with EZH2 inhibitor GSK126 (5μM, #15415, Cayman Chemicals) for 7 days before analysing by western blot. Recombinant lentivirus production and

transduction were described earlier (2). Transduced A549 cells were selected with 5μg/ml blasticidin (15205, Sigma-Aldrich).

Real-Time Quantitative Polymerase Chain Reaction. Total RNA of lung tumor samples were isolated as described earlier (1). Reverse transcription and quantitative real-time polymerase chain reaction (qRT-PCR) were described earlier (2), with primers listed below. Relative messenger RNA (mRNA) levels were calculated relative to mouse ß-actin.

Mm_Bactin_Fwd:	CTAAGGCCAACCGTGAAAAG
Mm_Bactin Rev:	ACCAGAGGCATACAGGGACA
Mm_B2m_Fwd:	CCCGCCTCACATTGAAATCC
Mm_B2m_Rev:	TCACATGTCTCGATCCCAGT
Mm_Nlrc5_Fwd:	CAGCTATGAGCCCTCCAACC
Mm_Nlrc5_Rev:	GTTTGGCACCATGGTACAGC
Mm_H2-D1_Fwd:	TGAGGAACCTGCTCGGCTACTA
Mm_H2-D1_Rev:	GGTCTTCGTTCAGGGCGATGTA
Mm_H2-K1_Fwd:	GGCAATGAGCAGAGTTTCCGAG
Mm_H2-K1_Rev:	CCACTTCACAGCCAGAGATCAC
Mm_H2-T23_Fwd:	CTCGCTGCGGTATTTCACCA
Mm_H2-T23_Rev:	AGCGTGTGAGATTCGTCGT

Recombination measurements and PCR. Tumor and adjacent tissue samples were dissected from PFA fixed lungs, and purified DNA using QIAamp DNA FFPE Tissue Kit (QIAGEN, 56404). The PCR reactions were prepared with the following contents: 100ng genomic DNA, 5μM of each PCR primer listed as below, GoTaq DNA polymerase (Promega, M3005) and H2O. PCR condition of KrasG12D: 95°C-5 min, 95°C-30 sec, 61°C-30 sec, 72°C-45 sec, 35 cycles, 72°C-10

min, 4°C-hold. PCR condition of AMPK flox and recombined alleles: 95°C-5 min, 95°C-30 sec, 58°C-30 sec, 72°C-10 sec, 35 cycles, 72°C-2 min. 4°C-hold.

*KrasG12D*_Primer 1:	GTCTTTCCCCAGCACAGTGC
*KrasG12D*_Primer 2:	CTCTTGCCTACGCCACCAGCTC
*KrasG12D*_Primer 3:	AGCTAGCCATGGCTTGAGTAAGTCTGCA
AMPKα1_flox_Fwd:	AATAGCCCATGAGCTCCAGA
AMPKα1_flox_Rev:	TGCAGCCCTACACTGAAATG
AMPKα2_flox_Fwd:	ATGGCTTGGCGCTGTCTA
AMPKα2_flox_Rev:	ACTTTCTGGCCAGGCAGATG
AMPKα1_rec_Fwd:	CCCATGAGCTCCAGAAGAAG
AMPKα1_rec_Rev:	GCCAGACACAGGTGAAGACA
AMPKα2_rec_Fwd:	GATCTGTCTGCTTCTGCGTTC
AMPKα2_rec_Rev:	CGATGGCCGCTCTAGATAAC

Gene set enrichment analysis

The gene set enrichment analysis (GSEA) (https://www.gsea-msigdb.org/gsea/index.jsp) was performed on fold-change ranked expressed genes in human *KL* TCGA LUAD datasets and mouse *KL* and *KAA* datasets. For the pAMPKα in TCGA LUAD dataset, Spearman correlation coefficient was used as a ranking criteria. For PRC2-related gene sets, ranked lists for human and mouse RNA-sequencing results were probed against BENPORATH_PRC2_TARGETS, BENPORATH_SUZ12_TARGETS and BENPORATH_EED_TARGETS. The results were visualized and interpreted using ggplot2 package in R (v3.6.2).

Cancer Cell Line Encyclopedia. We focused on the analysis of non-small cell lung cancer cell lines. Reads per kilobase per million (RPKM) values for *B2M* were obtained from Broad Institute

Cancer Cell Line Encyclopedia data portal (CCLE portal, https://portals.broadinstitute.org/ccle).

Mutation statuses for *KRAS* and *LKB1* were obtained from cBioportal.

Reference:

1. Gao Y, Yan Y, Tripathi S, Pentinmikko N, Amaral A, Päivinen P, et al. LKB1 Represses ATOH1 via PDK4 and Energy Metabolism and Regulates Intestinal Stem Cell Fate. Gastroenterology 2020; 158: 1389-1401.e10.
2. Yan Y, Ollila S, Wong IP, Vallenius T, Palvimo JJ, Vaahtomeri K, et al. SUMOylation of AMPKalpha1 by PIAS4 specifically regulates mTORC1 signalling. Nat Commun 2015; 6: 8979.
3. Vaahtomeri K, Ventelä E, Laajanen K, Katajisto P, Wipff PJ, Hinz B, et al. Lkb1 is required for TGFβ-mediated myofibroblast differentiation. J Cell Sci 2008; 121: 3531-3540.